

## Characterization of Future Rainfall Prone to Sediment Hazards in a Changing Climate Using Radial-Basis Function Network: A Case Study of Rokko Mountain Area

Ying-Hsin WU, Akihiko YAMAJI and Eiichi NAKAKITA

### Synopsis

This study, as a first attempt, aims to utilize the method of Radial-Basis Function Network (RBFN) to examine hourly rainfall intensity and soil-water index obtained from climate projections for investigating features of future rainfall under climate change influences. Our study area is focused on Rokko Mountain in Hyogo prefecture. The 1-km MLIT 3rd-mesh system is adopted in our analysis. The 2-km and 5-km Non-Hydrostatic Regional Climate Models (NHRCM) under RCP2.6 and RCP8.5 scenarios are used as future climate projections. A transformation matrix is used to quantify geometrical changes of RBFN contours. The characteristics of cumulative rainfall amount and rainfall duration of hazardous rainfall events are also examined. The analysis results show that soil-water index is much enlarged while hourly rainfall is a bit enlarged under RCP2.6, but, reversely, soil-water index remains unchanged while hourly rainfall is much intensified on the mountain side facing Osaka Bay under RCP8.5 in 2-km NHRCM. The hazardous rainfall events in 2-km NHRCM have shorter durations and smaller cumulative amount comparing to the ones in 5-km NHRCM.

**Keywords:** climate change, NHRCM, Radar-AMeDAS, Radial Basis Function Network

### 1. Background

In the last decades, extreme climate becomes more frequent to trigger considerable severe water-related disasters and has raised the great attention of the government authorities and scientific communities. Recent extreme rainfall events show obvious changes that rainfall was elongated in the period and intensified in a much higher accumulated amount and peak intensity that have broken new observation records in many places, and have triggered devastating floods, landslides, and sediment disasters beyond our experience. IPCC report (IPCC, 2021) shows an increasing trend of global temperature on earth-surface over the last 50 years, and this increasing trend is termed as global warming phenomenon due to the huge amount of emissions of greenhouse from human industrial

development in the last century. Under the influences of global warming phenomenon in Japan, long-term observation (JMA, 2020) has revealed an increasing trend of occurrence frequency of extreme rainfall of which the hourly precipitation is greater than 80 mm, and, meanwhile, a decreasing trend of annual precipitation days. This implies that, in the future, it would be more likely to occur much intensified rainfall which is prone to amplify occurrence of landslides and sediment hazards. To achieve early warning practices for these kinds of hazards, Ministry of Land, Infrastructure, Transport and Tourism (abbreviated as MLIT) is currently applying critical line (CL) method which utilizes two hydrometeorological indices, i.e., hourly rainfall intensity (PREC hereafter) and soil-water index (SWI) (Osanai et al., 2010; MLIT 2020). The two hydrometeorological indices can reflect influences

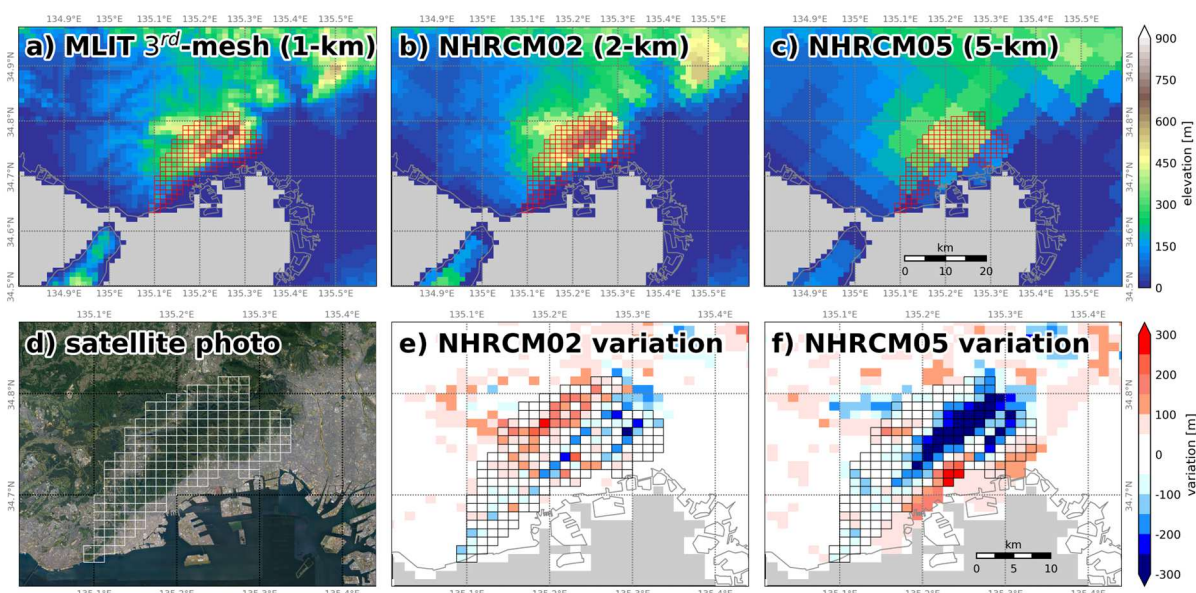


Fig. 1 Comparison among digital elevation models of MLIT 3rd-mesh (1-km), NHRCM02 (2-km), and NHRCM05 (5-km) in Subfigures a-c). Subfigure d) shows the study area of Rokko mountain. The elevation variation relative to MLIT 3rd-mesh DEM are shown in e) and f). The target meshes are denoted by white rectangles. The satellite photo is extracted from Google Map.

of short-term peak rainfall and long-term soil moisture condition on landslide occurrence and can be reasonably applied to assess potential risk of sediment disasters (Saito and Matsuyama, 2015). Also, we have explored the future changes of disastrous rainfall prone to sediment disasters (Wu et al., 2020; 2021; 2022). However, we only considered the values of maximum PREC and SWI without examining overall features of the two rainfall indices. Therefore, we herein attempt to investigate future changes of PREC and SWI with a focus on the maximal geometric range of the two indices. For future climate projection, we adopted the 2-km and 5-km Non-Hydrostatic Regional Climate Models, which is often called NHRCM (Murata et al., 2015; Murata et al., 2017; Kawase et al., 2021; Murata et al., 2022) and published by Meteorological Research Institute (MRI) of Japan Meteorological Agency (JMA). Hereafter, the two RCMs are abbreviated as RCM2 and RCM5, respectively. The 1-km reanalyzed precipitation data is used for verification. To reveal the geometrical change of the two rainfall indices on each 1-km MLIT 3rd-mesh, we utilize Radial Basis Function Network (RBFN) (Osanaï et al., 2010) to quantify the geometrical distribution of the two indices and

examine stretching of RBFN curves among scenarios to interpret its relation to future changes of rainfall prone to sediment disasters.

In this study, we select Rokko Mountain in Hyogo prefecture as our study area, as is shown in Fig. 1. In what follows, the introduction to data and methodology we used will be mentioned in Section 2, the analysis results will be discussed in Section 3. The final part of Section 4 is concluding remarks.

## 2. Data and Method

### 2.1 JMA Radar-AMeDAS

For verification and comparison, we utilized high-resolution precipitation reanalyzed using observations of 20 C-band radars and the Automated Meteorological Data Acquisition System (abbreviated as AMeDAS) operating by JMA. The data period is from 2006 to 2022 (17 years in total). The resolutions are 30 minutes in time and 1 square kilometer in space. As one of the major benefits, the coordinate system used for Radar-AMeDAS is just the MLIT 3rd-mesh system which is using for early-warning of sediment disaster. This means that the data on each 1-km mesh can well represent the rainfall on that scale. For brevity, Radar-AMeDAS

dataset is herein abbreviated as JMARA.

## 2.2 Future climate projections NHRCM

The spatiotemporal resolutions of RCM5 are 5 km in space and 30 minutes in time, and RCM2 are 2 km in space and 1 hour in time. The differences of digital elevation models (DEM) among 1-km MLIT 3rd-mesh, 2-km RCM2, and 5-km RCM5 are illustrated in Fig. 1. The RCM2's DEM is similar to the real topographic, but the RCM5's rather differs from the real topographic that the mountain peak is smoothed out. Some belief information of the two RCM is listed in Table 1. Both have the same ensemble members, including one present climate projection SPA, and four ensemble members of future projections for the two scenarios of Representative Concentration Pathway (RCP) 2.6 and 8.5 proposed in IPCC Fifth Assessment Report in 2014 for representing human activities of industrial development. Each RCM is downscaled from the simulation of a global climate model MRI-AGCM3.2S by imposing sea-surface temperature (SST) of each scenario as the sea surface boundary condition. The four future SST patterns are related to El Niño phenomena. More technical details about the two RCM can refer to the literature (Murata et al., 2015; Murata et al., 2017; Kawase et al., 2021; Murata et al., 2022). The simulation period of each RCM is 20 years with a one-year time slice and a spin-up period of 43 days. For the sake of brevity, we shall take average of the four ensembles of RCP2.6 and RCP8.5 to discuss their average features.

## 2.3 Extraction of rainfall events and indices

In this study, the grid system of MLIT 3rd-mesh whose spatial resolution is 1 square kilometer is

adopted for analysis. We processed JMARA dataset continuously from 2006 to 2022 and processed the 20-year datasets of RCM5 and RCM2 in each one-year time slice. The procedures of extraction of rainfall events and indices are mentioned as follows. The first step was to directly extract continuous time series of rainfall on the center of each 1-km mesh without interpolation, and to convert the interval into 10-minute by uniformly distributing the original rainfall series in the interval of 30 minute or one hour. Then, the converted 10-minute rainfall series was used for calculating continuous time series of SWI by using the conventional method proposed by JMA. Referring to MLIT's definition of rainfall events (MLIT, 2020), we picked up all effective rainfall events with a minimal rainfall threshold of 0.5 mm/hr. The two obtained time series of PREC and SWI index were further analyzed to count occurrence times of hazardous rainfall by checking whether critical lines are passed as well as to identify change features of hazardous rainfall using the method of RBFN.

## 2.4 Radial-Basis Function Network (RBFN)

In the current early-warning system, the criteria, or called critical line on the parametric plane of rainfall indices, for predicting occurrence of sediment disaster are determined using the method of Radial Basis Function Network, which is often abbreviated as RBFN (MLIT, 2020; Osanai et al., 2010). For brevity, the RBFN theory is not detailed here. By using radial basis function, such as Gaussian basis function, RBFN is quite useful for function approximation problems in many fields. Therefore, the RBFN has been successfully used to quantify geometrical range of PREC and SWI of

Table 1 Brief information of all NHRCM members

Dataset	Scenario	Boundary SST	Simulation Period
SPA	N/A	Monthly observation (1979-2003)	from 1980/09/01 to 2000/08/30
SFA_C1	RCP2.6 & RCP8.5	Less warm in East tropical Pacific	from 2076/09/01 to 2095/08/30
SFA_C2		Stronger El Niño	
SFA_C3		Warmer in Northwest Pacific	
SFA_C0		El Niño	

SPA: present climate, SFA: future climate projection

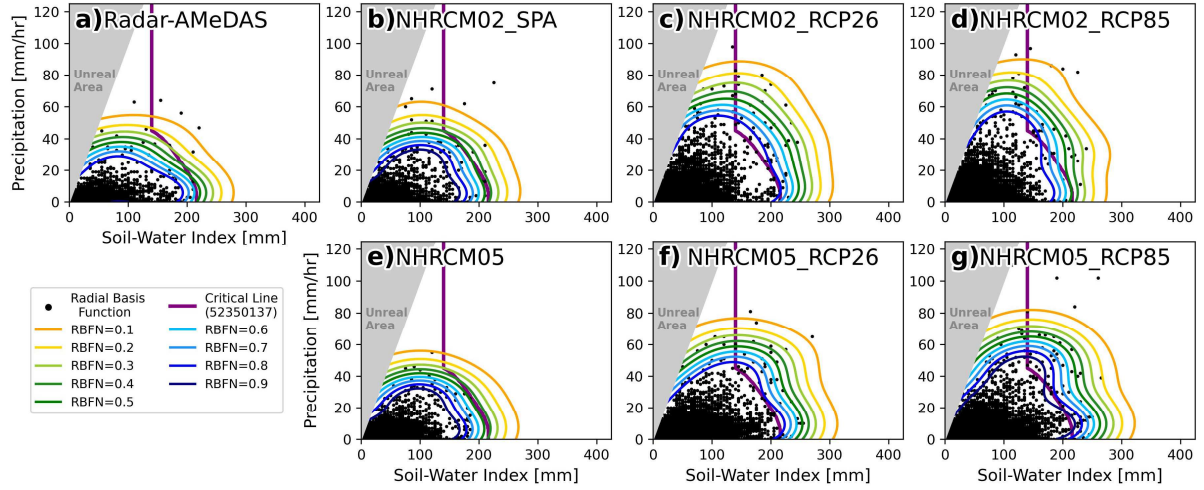


Fig. 2 Contours of the response surfaces of rainfall indices (hourly precipitation and soil-water index) using Radial Basis Function Network (RBFN) under the scenarios of (b, e) present climate, (c, f) RCP2.6, and (d, g) RCP8.5 as well as (a) historical observation at the mesh No. 52350137 where Kobe Meteorological Observatory is located. The analysis for RCP2.6 and RCP8.5 is performed by taking all the four members (C0, C1, C2, C3) into account.

non-occurrence rainfall events. To borrow this beneficial concept, as a first attempt, we utilize the method of RBFN to the indices from climate projections to examine future changes of rainfall indices under climate change influence. In our analysis, we follow the same theory and parameter settings to implement the RBFN model by referring to the official MLIT guideline (MLIT, 2020).

The input for training the RBFN model is pairs of rainfall indices, and the output of RBFN is a response surface representing a probability density function of non-occurrence rainfall. To gently remind, we only focus on investigating overall features of rainfall event on each mesh, but not on determining criteria of disaster occurrence. So, we consider all rainfall events are non-occurrence ones, and used them to RBFN for finding out corresponding response surfaces of rainfall events. Finally, we examined geometrical stretch of response surfaces among present and future projections to evaluate the future change of rainfall events.

## 2.5 Stretch of response surface of RBFN

After obtaining response surfaces using RBFN, we then characterized the geometrical change of response surface with a focus on examination of contours on the surface. Because sediment hazards

are usually triggered by extreme rainfall, our analysis tries to focus on this kind of rainfall which may occurred in a lower probability. As a response surface represent a probability density function of non-occurrence rainfall, we choose to examine the contour of  $RBFN = 0.1$  which can be reasonably considered as a boundary of extreme rainfall event. To quantify the geometrical change between the RBFN contours of present and future projections, we assume a linear transformation mapping of two contours,

$$X_i = Jx_i, \quad (1)$$

where  $x_i = (s_i, p_i)$  respectively denotes the sequences of SWI and PREC of SPA with  $n$  pairs for  $i = 1 \cdots n$ , and  $X_i = (S_i, P_i)$  denotes the ones of future projections SFA. The transformation matrix  $J$  is expressed as

$$J = \begin{bmatrix} A & B \\ C & D \end{bmatrix} = \begin{bmatrix} S_{SWI} \cos \varphi & -S_{SWI} \sin \varphi \\ S_{PREC} \sin \varphi & S_{PREC} \cos \varphi \end{bmatrix}, \quad (2)$$

where  $A$ ,  $B$ ,  $C$ , and  $D$  are the scaling component,  $S_{SWI}$  and  $S_{PREC}$  the scaling factors in the directions of SWI and PREC, respectively, and  $\varphi$  denotes the rotation angle with respect to the axes. In our analysis which will be explained later, the rotation angle  $\varphi$  is generally too small to be ignored

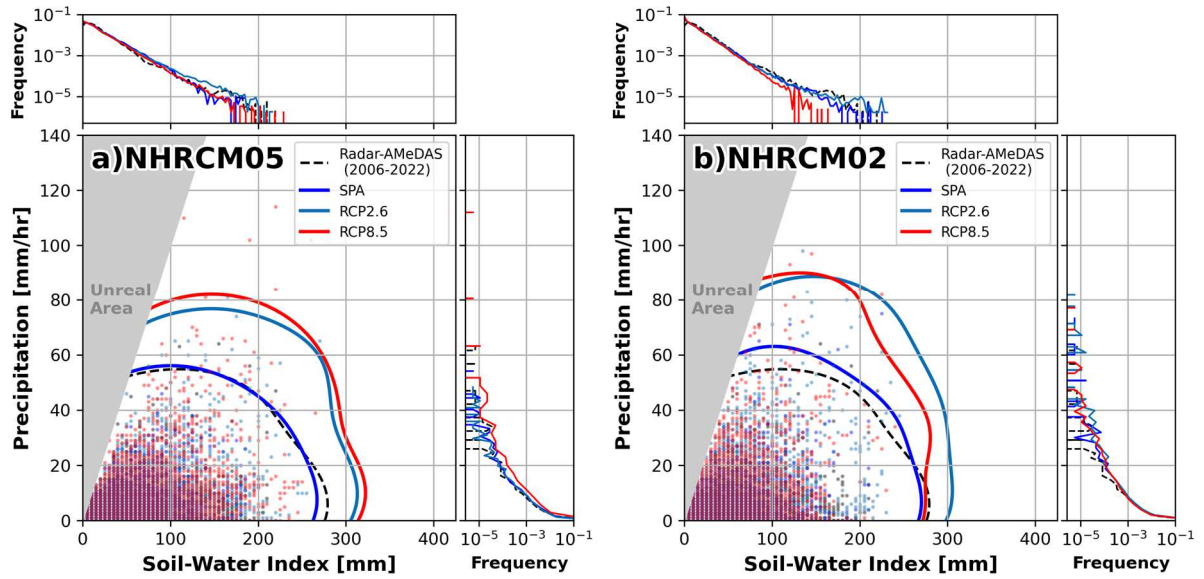


Fig. 3 Comparison of the contours of  $RBFN = 0.1$  under historical observation and the three climate scenarios from a) NHRCM05 and b) NHRCM02 on the same mesh No. 52350137. The upper and right subfigures show the relative frequency of all events' Soil-Water Index and Precipitation. Each circles denote information from rainfall events.

hereafter. By comparing between contours of future climate with respect to the present climate, with the stretch ratios  $S_{SWI}$  and  $S_{PREC}$ , a contour can be considered as being expanded in the positive SWI direction if  $S_{SWI} > 1$ , and shrunk in the negative SWI direction when  $S_{SWI} < 1$ . The similar manner is also applied to  $S_{PREC}$ . Then, the least squares method is then used to determine the four scaling components of  $A$ ,  $B$ ,  $C$ , and  $D$ . The exact formulas are listed in the appendix. With the obtained  $J$ , further algebra gives the scaling factors of  $S_{SWI}$  and  $S_{PREC}$  for quantification of the stretch or shrink of the shape of RBFN contours.

### 3. Analysis and Discussion

#### 3.1 Comparison with Radar-AMeDAS

Fig. 2 illustrates comparison among the historical observation of JMARA, and climate projections under different scenarios using RCM2 and RCM5 on the mesh of No. 52350137 where Kobe Meteorological Observatory is located. The contours in each dataset were obtained using corresponding trained RBFN models. As a result, the contour of SPA in RCM5 is similar to the JMARA

contour with a slight extension of SWI, but the one of RCM2 has a higher PREC. The contours of RCP2.6 in both RCMs show wider ranges of PREC and SWI comparing to SPA. The contours of RCP8.5 in RCM5 have a slightly wider than RCP2.6, but the ones of RCM2 are shrunk in the SWI axis. For better comparison, Fig. 3 overlays all the contours of  $RBFN = 0.1$  of all datasets from both RCMs with relative frequency of SWI and PREC of rainfall events. Clearly, we can see that the shape of  $RBFN = 0.1$  contour is highly related to the frequency of the two indices that the wider in the direction of a rainfall index a wider frequency range for the corresponding rainfall event, and vice versa. Also, the RBFN contours could infer the distributions with probability information.

#### 3.2 Future changes of hourly rainfall and Soil-Water Index

Fig. 4 illustrates the results of scaling ratios of  $S_{SWI}$  and  $S_{PREC}$  of future climate projection with respect to the present one. In the RCP2.6 scenario, the range of SWI is much expanded as most of  $S_{SWI} \geq 1$ , and the PREC is also much extended in RCM2 but slightly extended with some meshes

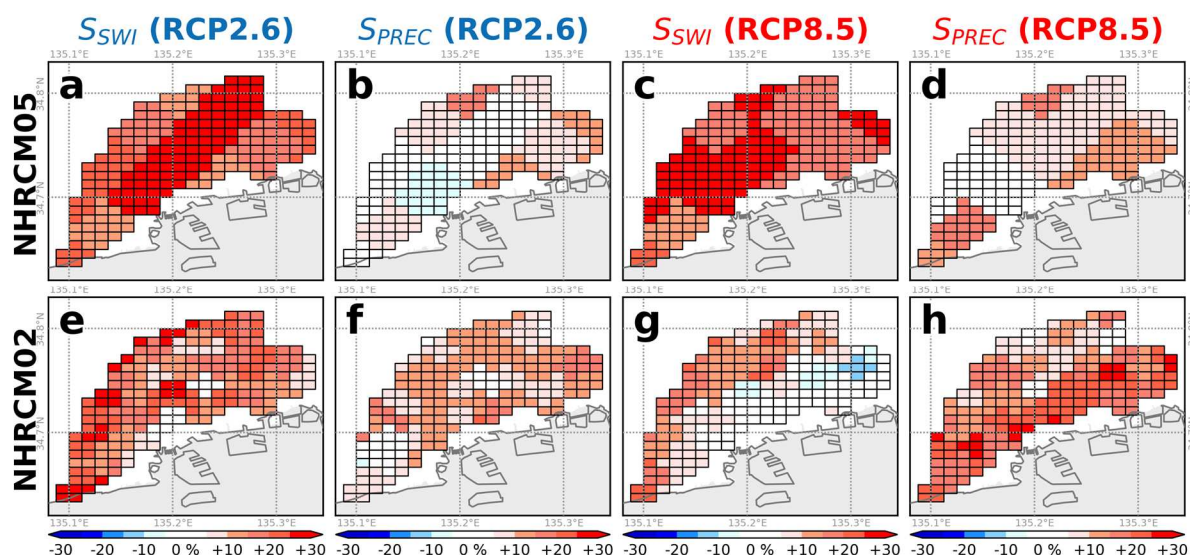


Fig. 4 The change ratios [%] of stretch of the contours of  $RBFN = 0.1$ , i.e.,  $S_{PREC}$  and  $S_{SWI}$ , under the future scenarios of RCP2.6 and RCP8.5 relative to the present climate member. The upper and lower rows show the results using 5-km and 2-km NHRCM.

shrunk as  $S_{SWI} < 1$  in RCM5. This indicates the rainfall pattern will tend to intensify the maximum of SWI in both RCMs but not to significantly change the maximum of PREC in RCM5. Moreover, in the RCP8.5 scenario, the contour feature is similar to the RCP2.6 with a bit extension in RCM5. Particularly, we find a reverse condition in RCM2 that the range of SWI is shrunk on the mountain side facing the Osaka Bay. However, on the same side, the range of PREC is much extended as  $S_{SWI} > 1.2$ . From this condition, we could infer that the rainfall pattern will be intensified to a higher hourly cumulative rainfall amount but weakened to decline the maximum SWI.

Regarding the spatial distribution of RCP8.5 in RCM2, we can observe that the stretch features are divided well by the mountain ridge of the real topography and the change of PREC is more obvious on the side of Rokko Mountain facing the Osaka Bay than the other side. This reason would be due to that the DEM of RCM2 matches better with the real topography, as is shown in Fig. 1. As noticing this opposite feature of the stretch of the ranges of SWI and PREC under RCP2.6 and RCP8.5, we performed further analysis to examine characteristics of rainfall events prone to disaster and corresponding disaster occurrence conditions, which will be explained in the next subsection.

### 3.3 Features of hazardous rainfall events

To reveal the relation between stretch features of contours and possible disaster risk, we extracted all disaster-prone rainfall events on each mesh by using each specific critical line. With the extracted hazardous events, we first examined the relation between cumulative rainfall amount and rainfall duration, as is shown in Fig. 5. Herein, all events are extracted based on rainstorm system. We can see the rainfall durations of RCM2 events are almost concentrated within 72 hours and the cumulative amount mainly ranges between 100 and 400 mm with an average of maximum intensity  $> 60$  mm/hr. Then, the duration of RCM5 events lasts longer until 240 hours (10 days), and the cumulative amount mainly ranges between around 150 and 600 mm with a maximum intensity  $< 20$  mm/hr. Particularly, in RCM5 there are totally 32 events with the maximum hourly in-tensity  $< 20$  mm/hr and the cumulative amount  $> 500$  mm. In these events the corresponding critical line is passed because of much higher SWI. On the other hand, the intensity of most RCM2 events is greater than 30 mm/hr, and there are fewer events under RCP8.5. This condition reflects the future climate events of RCM2 hold higher peak hourly rain rate, and the ones of RCM5 generally possess weaker hourly intensity and longer durations. Among influential factors, the major difference of

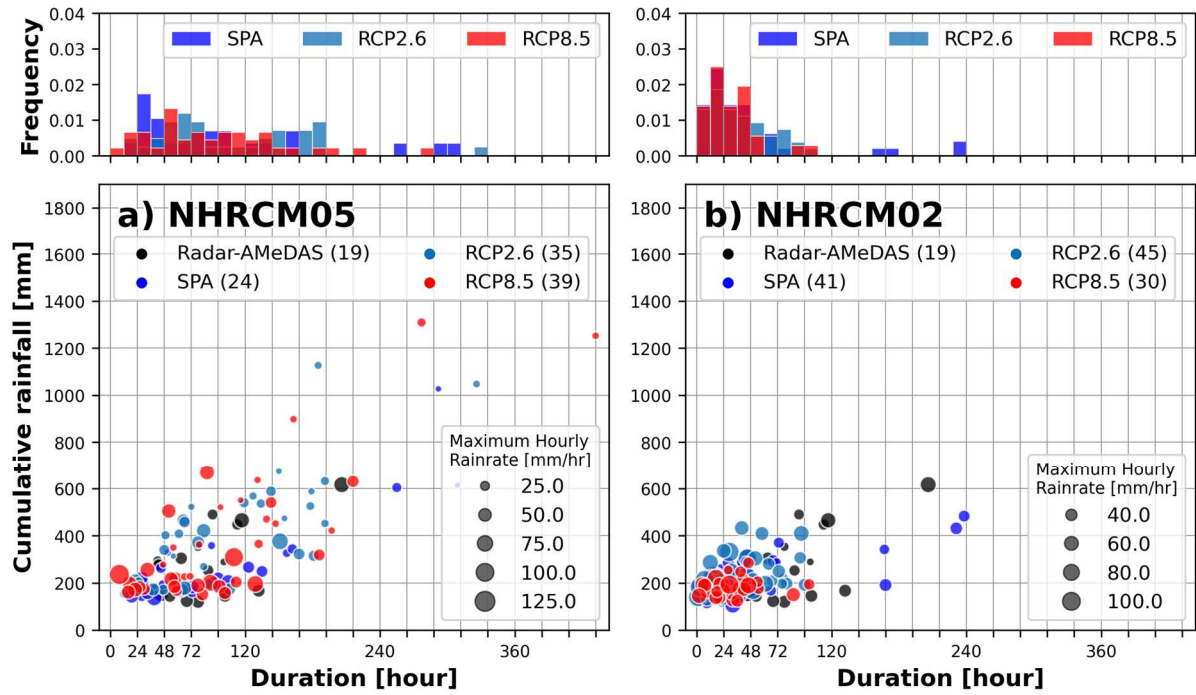


Fig. 5 Relation between cumulative rainfall and durations of the events passing CL and histograms with the bin width of 12 hours. The colors denote variable datasets. The date period of Radar-AMeDAS is 17 years and the others' are 20 years. The symbol size denotes the peak hourly rain rate. The event number is quoted after dataset item in the legend.

rainfall property between two RCMs could be attributed to the grid resolution of which the effect can also be seen from the stretch features, as is shown in Fig. 4.

Regarding the hazard occurrence condition, Fig. 6 shows the maps of hazardous rainfall event counts and the monthly frequency. Without significant difference of monthly frequency between two RCMs, the maps of RCM2 show decreasing trends in future projections, as are shown in Figs. 6e and 6f. This decline trend can be verified by that the total number of SPA event is 1.7 times of the RCP8.5 one, shown in Fig. 4. Meanwhile, it has been reported in the literature (Murata et al., 2022) that in the area near Osaka Bay the 20-yr mean maximum hourly precipitation in July and August is higher in the present climate than the future one. This also verifies that RCM2 holds decreasing future trends as higher hourly precipitation will accompanies higher possibility of hazard occurrence. More efforts will be needed to clarify the mechanism of rainfall generation in this area under present and future climate scenarios.

#### 4. Concluding remarks

In this study, we investigated future changes of rainfall prone to sediment hazards by quantifying the geometrical stretching of RBFN contours of rainfall indices, i.e., soil-water index SWI and hourly precipitation PREC, obtained from 5-km and 2-km NHRCM. We also revealed the relation among the stretch features of RBFN contours, the basic property of hazardous rainfall events, and possible disaster risk. The characteristics of cumulative rainfall amount and rainfall duration of hazardous rainfall events are also examined. The analysis results show that soil-water index is much enlarged while hourly rainfall is a bit enlarged under RCP2.6, but, reversely, soil-water index remains unchanged while hourly rainfall is much intensified on the mountain side facing Osaka Bay under RCP8.5 in 2-km NHRCM. Regarding hazardous rainfall characteristics, the hazardous rainfall events in 2-km NHRCM have shorter durations and smaller cumulative amount comparing to the ones in 5-km NHRCM.

This study demonstrates the applicability of

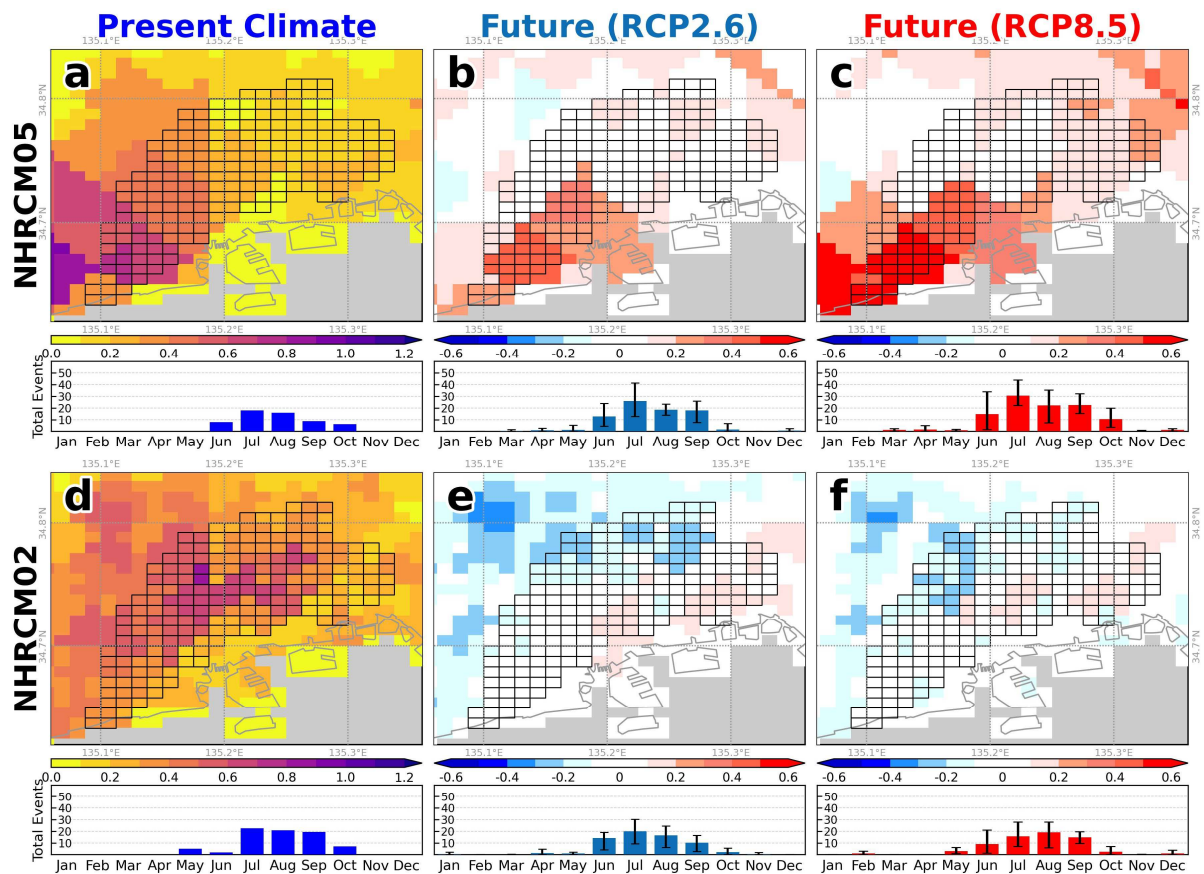


Fig. 6 The spatial distribution and mesh-based monthly frequency of hazardous rainfall events under the scenarios of SPA (a, d), RCP2.6 (b, e), and RCP8.5 (c, f). The values of SPA denote cumulative counts, and the values of RCP2.6 and RCP8.5 denote variation relative to SPA. The upper and lower rows show the results using 5-km and 2-km NHRCM.

RBFN with a Jacobian transformation matrix to assess the future change of rainfall events and provide an alternative and objective way which can systematically quantify characteristics of hazardous rainfall in the future under climate change impact. Furthermore, the quantified future changes of snake line on each 3rd-mesh can help identify possible hazardous rainfall pattern to assess future sediment hazards.

#### Acknowledgements

The datasets of 2-km and 5-km NHRCM are provided by the Integrated Research Program for Advancing Climate Models (TOUGOU) Grant Number JPMX-D0717935498 from the Ministry of Education, Culture, Sports, Science and Technology (MEXT), and by Research Funding from MLIT Rokko Sabo Office, and by JSPS KAKENHI Grant

Number 22K04331. We appreciate MLIT Sabo Planning Division, Rokko Sabo Office, Hyogo prefectural government, and Japan Weather Association (JWA) for sharing valuable datasets. The authors are grateful to the Publishing Committee members who made the previous versions of this instruction.

#### References

- IPCC (2021): Climate Change: The Physical Science Basis. Contribution of Working Group I to the Sixth Assessment Report of the Intergovernmental Panel on Climate Change.
- Japan Meteorological Agency (2020): Climate Change in Japan.
- Kawase, H., Murata, A., Yamada, K., Nakaegawa, T., et al. (2021): Regional characteristics of future

changes in snowfall in Japan under RCP2.6 and RCP8.5 scenarios, SOLA, Vol. 17, pp. 1–7.

MLIT (2020): Committee Discussions on Technology and Evaluation of Sediment Disasters under Climate Change. (in Japanese)

Murata, A., Sasaki, H., Kawase, H., Nosaka, M., et al. (2015): Projection of future climate change over Japan in ensemble simulations with a high-resolution regional climate model. SOLA, Vol. 11, pp. 90–94.

Murata, A., Sasaki, H., Kawase, H., Nosaka, M., et al. (2017): Projection of future climate change over Japan in ensemble simulations using a convection-permitting regional climate model with urban canopy. SOLA, Vol. 13, pp. 219–223.

Murata, A., Nosaka, M., Sasaki, H. and Kawase, H. (2022): Dynamic and thermodynamic factors involved in future changes in extreme summertime precipitation in Japan projected by convection-permitting regional climate model simulations, JAMC, Vol. 61(9), pp.1221–1237.

Osanai, N., Shimizu, T., Kuramoto, K., Kojima, S. and Noro, T. (2010): Japanese early-warning for debris flows and slope failures using rainfall indices with Radial Basis Function Network, Landslides, Vol. 7, pp. 325–338.

Saito, H. and Matsuyama, H. (2015): Probable Hourly Precipitation and Soil Water Index for 50-yr Recurrence Interval over the Japanese Archipelago, SOLA, Vol. 11, pp. 118–123.

Wu, Y.-H., Nakakita, E. and Yamaji, A. (2022): Scaling of snake line change based on Clausius-Clapeyron Relation. J. Jpn. Soc. Civ. Eng., Ser.

B1 (Hydraulic Eng.), 78(2), pp. I\_97–I\_102.

Wu, Y.-H., Nakakita, E. and Yamaji, A. (2021): Future change of snake line pattern and its relation to sediment disasters, J. Jpn. Soc. Civ. Eng., Ser. B1 (Hydraulic Eng.), Vol. 77(2), pp. I\_193–I\_198.

Wu, Y.-H., Nakakita, E. and Kunitomo, M. (2020): Future change of rainfall-triggered landslide risk using NHRCM05 based on critical line method, J. Jpn. Soc. Civ. Eng., Ser. B1 (Hydraulic Eng.), Vol. 76(2), pp. I\_67–I\_72, 2020.

## Appendix

Using the least-square method, the exact equations for determining each component in  $J$  are given as below,

$$A = \frac{\sum p_i s_i \cdot \sum p_i s_i - \sum s_i s_i \cdot \sum p_i p_i}{(\sum s_i p_i)^2 - \sum s_i s_i \cdot \sum p_i p_i}, \quad (1)$$

$$B = \frac{\sum p_i s_i \cdot \sum s_i s_i - \sum s_i s_i \cdot \sum s_i p_i}{\sum s_i s_i \cdot \sum p_i p_i - (\sum s_i p_i)^2}, \quad (2)$$

$$C = \frac{\sum p_i p_i \cdot \sum p_i s_i - \sum p_i s_i \cdot \sum p_i p_i}{(\sum s_i p_i)^2 - \sum s_i s_i \cdot \sum p_i p_i}, \quad (3)$$

$$D = \frac{\sum p_i p_i \cdot \sum p_i s_i - \sum p_i s_i \cdot \sum p_i p_i}{\sum s_i s_i \cdot \sum p_i p_i - (\sum s_i p_i)^2}, \quad (4)$$

where  $\sum(\cdot)$  denotes the sequence summation of the series of parameter.

**(Received August 31, 2023)**